Matter and Radiation at Extremes

RESEARCH ARTICLE

scitation.org/journal/mre

Inverse Faraday effect of weakly relativistic full Poincaré beams in plasma

Cite as: Matter Radiat. Extremes 8, 014405 (2023); doi: 10.1063/5.0120072
Submitted: 11 August 2022 • Accepted: 16 December 2022 •
Published Online: 5 January 2023

Wei Liu,[1] Qing Jia,[1,a)] and Jian Zheng[1,2]

AFFILIATIONS

[1] Department of Plasma Physics and Fusion Engineering, University of Science and Technology of China, Hefei, Anhui 230026, People's Republic of China

[2] Collaborative Innovation Center of IFSA, Shanghai Jiao Tong University, Shanghai 200240, People's Republic of China

[a)] **Author to whom correspondence should be addressed:** qjia@ustc.edu.cn

ABSTRACT

The inverse Faraday effect (IFE), which usually refers to the phenomenon in which a quasi-static axial magnetic field is self-generated when a circularly polarized beam propagates in a plasma, has rarely been studied for lasers with unconventional polarization states. In this paper, IFE is reconsidered for weakly relativistic full Poincaré beams, which can contain all possible laser polarization states. Starting from cold electron fluid equations and the conservation of generalized vorticity, a self-consistent theoretical model combining the nonlinear azimuthal current and diamagnetic current is presented. The theoretical results show that when such a laser propagates in a plasma, an azimuthally varying quasi-static axial magnetic field can be generated, which is quite different from the circularly polarized case. These results are qualitatively and quantitatively verified by three-dimensional particle-in-cell simulations. Our work extends the theoretical understanding of the IFE and provides a new degree of freedom in the design of magnetized plasma devices.

I. INTRODUCTION

In laser plasma physics, quasi-static self-generated magnetic fields play important roles in particle acceleration,[1–4] photon emission,[5] laser fusion,[6–10] and other high-energy-density processes.[11–14] Among the mechanisms for the generation of quasi-static magnetic fields, the inverse Faraday effect (IFE) is of particular importance. The IFE usually refers to the phenomenon in which a quasi-static axial magnetic field is self-generated when a circularly polarized beam propagates in a plasma. Since its first observation in a plasma,[15] the IFE has been widely studied, and a number of explanations of this phenomenon have been proposed.[16–30]

In early work, IFE was explained using a magnetic dipole moment model,[16] in which the strength of the magnetic field is proportional to the electron number density, since electron motion is circular in a circularly polarized laser. This phenomenological model was developed further through the incorporation of collisionless cold electron fluid equations.[17–21] According to this nonlinear beating current model, when the electromagnetic waves are circularly polarized, the gradients in both plasma density and laser intensity will result in a nonlinear azimuthal current,[17] which leads to the generation of an axial magnetic field. When the electromagnetic waves are linearly polarized, this current will disappear, and no magnetic field will be generated. Since this nonlinear azimuthal current is generated by the electron quiver velocity beating with the high-frequency density perturbation, the generated magnetic field will dissipate quickly when the laser is no longer present. In Refs. 18–20, the effect of the diamagnetic current was taken into account through the introduction of conservation of generalized vorticity.[31] The results of the nonlinear beating current model were compared with those of particle-in-cell (PIC) simulations in Ref. 21.

When laser absorption and the accompanying angular momentum (AM) transfer are taken into account, it is found that linearly polarized beams can also lead to the generation of axial magnetic fields,[22] in contrast to the predictions of the nonlinear beating current model. It is known that a circularly polarized laser carries spin angular momentum (SAM).[32] When electromagnetic waves are absorbed by a plasma, the SAM of the waves will be transferred to the plasma, leading to the generation of an axial magnetic field.[23–26] As pointed out by Allen *et al.*,[33] laser beams with Laguerre–Gaussian

(LG) modes carry orbital angular momentum (OAM), and Ali *et al.*[22] explained how the axial magnetic field was generated due to OAM transfer during laser absorption. Recent advances in laser technology[34–38] have enabled the production of laser beams possessing intense OAM, which, with account taken of laser absorption, indicates that there is significant self-generation of magnetic fields by these LG beams.[27–30,39] Nuter *et al.*[29] found that when an intense (10^{18} W/cm^2) radially polarized laser propagates in a plasma, the AM of the laser can be transferred to the plasma without any dissipative effect, and a megagauss quasi-static axial magnetic field can be generated. This nondissipative AM absorption was further found to be caused by a process resembling direct laser acceleration, which is significant for intense lasers.[39] Longman and Fedosejevs[30] explored the spatial and temporal evolutions of magnetic fields driven by ultrahigh-intensity (10^{20} W/cm^2) beams carrying AM, and demonstrated the generation of kilotesla magnetic fields that persisted for several picoseconds after the laser had left the plasma.

In comparison, the nonlinear beating current mechanism[18–20] may be dominant in the presence of large plasma density gradients, such as in plasma channels,[19] and the IFE mechanism based on AM absorption[22,23,25,26] may become important when significant AM is transferred from laser beam to plasma.[29,30] It should be noted that almost all the previous studies[27–30] of magnetic fields generated by LG beams were based on AM absorption theory, with little attention being paid to the nonlinear beating current model.[18–20] It is unclear whether LG beams can generate axial magnetic fields when AM absorption is negligible. Besides, laser beams can possess unconventional polarization states, as in the case of full Poincaré (FP) beams,[40–43] which contain all the possible laser polarization states on the surface of the Poincaré sphere. We are interested in whether such a laser can generate an axial magnetic field when propagating in a plasma, and the possible distribution of the magnetic field as well as its relation to the polarization states is also of interest.

In this paper, based on the nonlinear beating current model,[18–20] the IFE of weakly relativistic linearly and circularly polarized LG beams is reconsidered, and the IFE of weakly relativistic FP beams is investigated in detail. Starting from the cold electron fluid equations and the conservation of generalized vorticity, an integrated theoretical model that takes into account the polarization states and LG modes is developed. The theoretical results show that for linearly polarized LG beams, no axial magnetic field can be generated. For circularly polarized LG beams, although axial magnetic fields can be generated, these fields are related only to the laser intensity, not to the helical phase structure of the LG beams. For FP beams that can be constructed by applying different azimuthal modes of LG beams on the two orthogonal polarizations,[40] azimuthally varying axial magnetic fields can be generated, which is quite different from the circularly polarized case. The structures of such magnetic fields are affected mainly by the LG mode difference Δl and the initial phase difference $\Delta\varphi$ of the two orthogonally polarized beams forming the FP beam. We also perform three-dimensional (3D) PIC simulations. To enable accurate comparisons of the simulation and theoretical results and keep other IFE mechanisms out of play, special care is taken in making the following choices of parameters: a long pulse with moderate intensity (5×10^{16} W/cm^2) is considered to interact with a cold plasma (10 eV, 1.1×10^{20} cm^{-3}), with the effects of collisions and parametric instabilities being neglected. The simulation results verify the theoretical results in terms of the distribution of magnetic fields, the distribution of source currents, and the conservation of generalized vorticity. In addition, it is noted that an axial magnetic field with arbitrary azimuthal distribution can be obtained if the polarization distribution of the constituent laser is properly designed using the linear superposition method. This provides a new azimuthal degree of freedom for magnetized plasma devices.[37,44–46]

The rest of the paper is organized as follows. In Sec. II, the theoretical model and corresponding results are given. In Sec. III, 3D PIC simulations are conducted to verify the corresponding theoretical results. In Sec. IV, we provide an intuitive explanation of these results and demonstrate a method for obtaining an arbitrary azimuthal distribution of the axial magnetic field. Conclusions are presented in Sec. V.

II. THEORETICAL MODEL

Electromagnetic waves propagating in the x direction can be expressed as $\mathbf{E}_L = g(x-ct)[E_y(x,y,z)\mathbf{e}_y + E_z(x,y,z)\mathbf{e}_z]\exp[i(k_0x-\omega_0t)]$, where k_0 and ω_0 are the laser wavenumber and frequency in vacuum, respectively, c is the speed of light in vacuum, $g(x-ct)$ is the laser temporal envelope and is assumed to be constant, $E_{y,z}(x,y,z)$ are the complex amplitudes with their respective polarizations, and $\mathbf{e}_{y,z}$ are the unit vectors in the y,z directions. The laser pulse duration is assumed to be shorter than ω_{pi}^{-1} (where ω_{pi} is the ion plasma frequency), so that the motion of ions can be neglected, and longer than ω_{pe}^{-1} (where ω_{pe} is the electron plasma frequency), so that the longitudinal variation can be neglected. The laser beams are assumed to be weakly relativistic $|E_{y,z}|/E_0 \ll 1$ ($E_0 = m_e\omega_0c/e$, where m_e is the electron mass and e is the elementary charge), so that the AM absorption described in Refs. 29, 30, and 39 can be ignored (a detailed discussion is provided in the Appendix).

We begin with the cold relativistic electron fluid equations and Maxwell equations

$$\frac{\partial n}{\partial t} + \nabla\cdot(n\mathbf{u}) = 0, \tag{1}$$

$$\left(\frac{\partial}{\partial t} + \mathbf{u}\cdot\nabla\right)(\gamma_0 m_e\mathbf{u}) = -e(\mathbf{E}+\mathbf{u}\times\mathbf{B}), \tag{2}$$

$$\nabla\times\mathbf{B} = \mu_0\varepsilon_0\frac{\partial\mathbf{E}}{\partial t} - \mu_0 ne\mathbf{u}, \tag{3}$$

$$\nabla\cdot\mathbf{E} = \frac{e}{\varepsilon_0}(n_0-n), \tag{4}$$

where n and $\mathbf{u}$ are the electron number density and velocity, respectively, $\mathbf{E}$ and $\mathbf{B}$ are the electric and magnetic fields, respectively, n_0 is the ion number density, which is equal to the initial electron number density for H-like plasmas, and $\gamma_0 \approx \sqrt{1+|\mathbf{E_L}|^2/(2E_0^2)}$ is the Lorentz factor averaged over the laser period. These variables can be decomposed into relatively low- and high-frequency (laser

frequency) components, which are denoted by subscripts s and f, respectively.

The low-frequency component of Eq. (3) describes the generation of the quasi-static magnetic fields and can be written as

$$\nabla \times \mathbf{B}_s = \mu_0 \varepsilon_0 \frac{\partial \mathbf{E}_s}{\partial t} - \mu_0 e \langle n_f \mathbf{u}_f \rangle - \mu_0 e n_s \mathbf{u}_s. \tag{5}$$

Here, the angle brackets represent averaging over the laser period. The right-hand side of Eq. (5) indicates three possible sources for the generation of a quasi-static magnetic field. $\mathbf{E}_s$ in the first term comes mainly from the charge separation field caused by the laser ponderomotive force. When the laser propagates steadily, this electric field hardly changes with time, and the first term can therefore be ignored. In the second term, $\mathbf{J}_{nl} = -e\langle n_f \mathbf{u}_f \rangle$ is a second-order nonlinear current as described in Refs. 17–21. The third term $\mathbf{J}_{dm} = -en_s\mathbf{u}_s$ represents the diamagnetic current resulting from the diamagnetic effect in response to the magnetic field generated by the nonlinear current in the second term. Applying conservation of generalized vorticity[31] and combining the high-frequency components of Eqs. (1)–(3), we can obtain the form of $\mathbf{J}_{nl}$ and the differential equation satisfied by $\mathbf{J}_{dm}$, from which the distribution of the self-generated magnetic field can be calculated accordingly.

First, $\mathbf{J}_{nl}$ can be obtained from the high-frequency components of Eqs. (1)–(3), which can be written as

$$\frac{\partial n_f}{\partial t} + \nabla \cdot (n_s \mathbf{u}_f) = 0, \tag{6}$$

$$\gamma_0 m_e \frac{\partial \mathbf{u}_f}{\partial t} = -e(\mathbf{E}_f + \mathbf{u}_f \times \mathbf{B}_s), \tag{7}$$

$$\nabla \times \mathbf{B}_f = \mu_0 \varepsilon_0 \frac{\partial \mathbf{E}_f}{\partial t} - \mu_0 n_s e \mathbf{u}_f. \tag{8}$$

Since the laser is weakly relativistic and the quasi-static self-generated magnetic field $\mathbf{B}_s$ is much weaker than the laser magnetic field, the high-frequency electron velocity satisfies $|u_f/c| \ll 1$ and $|\mathbf{u}_f \times \mathbf{B}_s|/|\mathbf{E}_f| = |u_f B_s|/|cB_f| \ll 1$. Thus, $\mathbf{u}_f \approx e\mathbf{E}_f/(i\omega_0\gamma_0 m_e)$ is obtained from Eq. (7). In addition, because the plasma is underdense, the amplitude of the laser field approaches that in vacuum, $\mathbf{E}_f \approx \mathbf{E}_L$. Equation (6) then gives $n_f = -e\nabla(n_s/\gamma_0) \cdot \mathbf{E}_L/(m_e\omega_0^2)$. Neglecting diffractive and refractive effects on the laser, we obtain $\mathbf{J}_{nl}$ in a cylindrical coordinate system as

$$\mathbf{J}_{nl} = -e\langle n_f \mathbf{u}_f \rangle = -\frac{e^3 (E_y E_z^* - E_y^* E_z)}{4i\gamma_0 m_e^2 \omega_0^3} \frac{\partial}{\partial r}\left(\frac{n_s}{\gamma_0}\right)\mathbf{e}_\theta, \tag{9}$$

where the asterisk * indicates the complex conjugate, and $n_s = n_0 + n_{\mathrm{pond}} = n_0 + \varepsilon_0 \nabla \cdot (\nabla |E_L|^2/\gamma_0)/(4m_e\omega_0^2)$, with n_{pond} being the density fluctuation induced by the laser ponderomotive force. Thus, if $\mathbf{J}_{nl}$ exists, it contains only a $\mathbf{e}_\theta$ component, which means that the self-generated magnetic field is mainly along the axis. For a weakly relativistic laser propagating in an initially uniform plasma, n_{pond} is usually relatively small, resulting in a self-generated magnetic field that is too weak to be detected in simulations. However, if there is an initial large density gradient $\partial n_0/\partial r$, the self-generated magnetic field can be significantly enhanced. In the following analysis, an initial nonuniform electron density will be applied to facilitate a clearer demonstration of the quasi-static magnetic field.

The other key current $\mathbf{J}_{dm}$ is determined mainly by $\mathbf{u}_s$. Since $\mathbf{u}_s$ is generated together with the magnetic field, it should be self-consistently calculated from the integral equation, taking account of the conservation of generalized vorticity. The electromagnetic fields $\mathbf{E}$ and $\mathbf{B}$ can be expressed in terms of potential fields $\mathbf{A}$ and φ as $\mathbf{E} = -\partial\mathbf{A}/\partial t - \nabla\varphi$ and $\mathbf{B} = \nabla \times \mathbf{A}$. Then, Eq. (2) can be rewritten as $\partial(\gamma_0 m_e \mathbf{u} - e\mathbf{A})/\partial t = \nabla(e\varphi - m_e c^2 \gamma) + \mathbf{u} \times [\nabla \times (\gamma_0 m_e \mathbf{u} - e\mathbf{A})]$, from which it follows that $\partial\boldsymbol{\omega}/\partial t = \nabla \times (\mathbf{u} \times \boldsymbol{\omega})$, where $\boldsymbol{\omega} = \nabla \times (\gamma_0 m_e \mathbf{u} - e\mathbf{A})$ is the generalized vorticity. Then, $\boldsymbol{\omega} = 0$ is always satisfied when we set the initial vorticity as zero in our model. The low-frequency part of $\boldsymbol{\omega}$ gives

$$\nabla \times (\gamma_0 m_e \mathbf{u}_s) = e\mathbf{B}_s. \tag{10}$$

Equation (10) is the differential equation satisfied by $\mathbf{u}_s$, which can be used to calculate $\mathbf{J}_{dm}$. It will be shown in the subsequent PIC simulations that this current always tends to weaken the magnetic field generated by $\mathbf{J}_{nl}$, which is why $\mathbf{J}_{dm}$ is regarded as a diamagnetic current.

Combining Eqs. (5), (9), and (10) and eliminating $\mathbf{u}_s$, we finally obtain the equation describing the generation of the axial magnetic field:

$$\nabla \times \left(\frac{\gamma_0}{n_s} \nabla \times \mathbf{B}_s\right) + \frac{\mu_0 e^2}{m_e} \mathbf{B}_s = \mu_0 \nabla \times \left(\frac{\gamma_0}{n_s} \mathbf{J}_{nl}\right). \tag{11}$$

From Eq. (11), it can be seen that the distribution of $\mathbf{B}_s$ is determined mainly by $\mathbf{J}_{nl}$ and n_s. Once n_s and $\mathbf{E}_L$ are known, the quasi-static axial self-generated magnetic field can be calculated.[18,20]

The above analysis is applicable to laser beams with different distributions and polarizations. In this paper, we focus mainly on laser beams with LG modes. Near the focal plane ($x = 0$), the complex amplitude of LG beams with $p = 0$ (where p is the radial index) can be written as

$$\begin{aligned} E^{LG}/E_0 &= a_0 h(r) \exp(il\theta + i\varphi) \\ &= a_0 C_l \left(\frac{r}{w_0}\right)^{|l|} \exp\left(-\frac{r^2}{w_0^2}\right) \exp(il\theta + i\varphi), \end{aligned} \tag{12}$$

where $h(r) = C_l (r/w_0)^{|l|} \exp(-r^2/w_0^2)$ is the beam radial distribution, l $(= 0, \pm 1, \pm 2, \ldots)$ is the azimuthal index, $r = \sqrt{y^2 + z^2}$, $\theta = \arctan(z/y)$, φ is the initial phase, a_0 is the dimensionless laser amplitude, and w_0 is the waist radius on the focal plane. C_l is a constant that ensures that different l modes of LG beams have the same maximum amplitude: $C_0 = 1$, and $C_l = (2e/|l|)^{|l|/2}$ when $l \neq 0$. LG beams have two unique features: one is the hollow amplitude distribution represented by $(r/w_0)^{|l|} \exp(-r^2/w_0^2)$, and the other is the helical phase structure represented by $\exp(il\theta)$.

For linearly polarized LG beams, $E_y^{LG}/E_z^{LG} = \mathrm{const}$. Equation (9) then gives $\mathbf{J}_{nl} = 0$, which means that no axial magnetic field can be

generated. For circularly polarized LG beams, $\mathbf{E}_L$ can be written as $E_z^{LG} = E_y^{LG} \exp(i\sigma_x\pi/2)$, where $\sigma_x = \pm 1$ represents right/left-hand circular polarization. Equation (9) can then be rewritten as

$$\mathbf{J}_{nl} = \frac{\sigma_x e^3 |E_y^{LG}|^2}{2\gamma_0 m_e^2 \omega_0^3} \frac{\partial}{\partial r}\left(\frac{n_s}{\gamma_0}\right)\mathbf{e}_\theta. \tag{13}$$

The sign of $\mathbf{J}_{nl}$ is determined by σ_x, which indicates that the direction of the self-generated axial magnetic field is opposite for different circular polarizations. The main features of the IFE given by this theory for LG beams are essentially consistent with those given in Refs. 17, 18, and 20 for linearly and circularly polarized Gaussian beams. These results are also demonstrated by 3D PIC simulations for Gaussian and LG beams in the Appendix.

The magnetic fields shown above are related only to the laser intensity $|E_y^{LG}|^2$, not to the helical index l. To introduce this helical index, we consider the case of FP beams,[40] which can be constructed by applying different $|l|$ modes of LG beams on the two orthogonal polarizations $E_{y,z}/E_0 = E_{y,z}^{LG}/E_0 = a_{y,z}h_{y,z}(r)\exp(il_{y,z}\theta + i\varphi_{y,z})$. Then, Eq. (9) can be rewritten as

$$\mathbf{J}_{nl} = -\frac{e^3 E_0^2 a_y a_z h_y(r) h_z(r)}{2\gamma_0 m_e^2 \omega_0^3} \frac{\partial}{\partial r}\left(\frac{n_s}{\gamma_0}\right)\sin(\theta\Delta l + \Delta\varphi)\,\mathbf{e}_\theta, \tag{14}$$

where $\Delta l = l_y - l_z$ and $\Delta\varphi = \varphi_y - \varphi_z$. When $\Delta l \neq 0$, Eq. (14) implies that $\mathbf{J}_{nl}$ varies with θ, which indicates that the self-generated magnetic field will also be associated with the azimuth θ. This feature is extremely different from the circular polarization case.

Figures 1(a)–1(d) display the transverse distributions of quasi-static axial magnetic fields calculated from Eqs. (11) and (14) for lasers with different polarization states propagating in a plasma. The initial density profile of the plasma is $n_{0,0} = n_{\rm ini}\exp[-(r/r_{\rm CH})^6]$, where $n_{\rm ini} = 0.1n_c$ and $r_{\rm CH} = 4\lambda$. Figure 1(a) shows the distribution of the axial magnetic field generated by a circularly polarized LG laser ($l_y = -1$, $l_z = -1$, and $\Delta\varphi = -\pi/2$), which is cylindrically symmetrical. Figure 1(b) shows the distribution of the axial magnetic field generated by a laser with $l_y = 1$, $l_z = -1$, and $\Delta\varphi = -\pi/2$. It can be seen that at a given r, the sign of the magnetic field changes four times as θ increases from 0 to 2π. Figure 1(c) shows the case for a laser with $l_y = 1$, $l_z = -1$, and $\Delta\varphi = 0$. Compared with Fig. 1(b), the magnetic field rotates through a certain angle around the axis, which demonstrates that the azimuthal distribution of the axial magnetic field can be changed by changing $\Delta\varphi$. Figure 1(d) shows the distribution of the magnetic field for a laser with $l_y = 2$, $l_z = -1$, and $\Delta\varphi = 0$, where the sign of the magnetic field changes six times azimuthally. The number of periodic changes in direction of the axial magnetic field is $N = 2\Delta l$, in accordance with that indicated in Eq. (14).

By constructing different l modes of LG beams on the two orthogonal polarizations, we introduce the helical index of LG beams into the magnetic field generation, which is reflected by azimuthal variation of the magnetic field. It is demonstrated that the distribution of the magnetic field is affected mainly by Δl and $\Delta\varphi$, which is quite different from the azimuthally homogeneous magnetic field generated by circular polarization. In Sec. III, we verify the above theoretical results by 3D PIC simulations.

III. 3D PIC SIMULATIONS

We perform a series of 3D kinetic simulations using the fully relativistic PIC code EPOCH.[47] The main simulation parameters are the same as those used in the above theoretical analysis. The laser

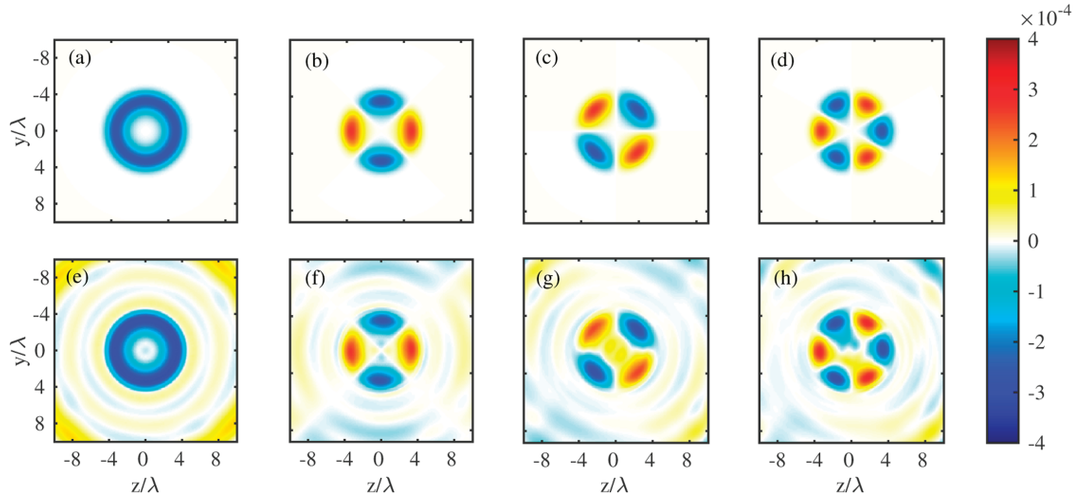

FIG. 1. Transverse distributions of the quasi-static axial self-generated magnetic fields (normalized by $B_0 = m_e\omega_0/e$) obtained from (a)–(d) the theoretical model and (e)–(h) 3D PIC simulations for lasers with different polarization states propagating in a plasma. The lasers have (a) and (e) $l_y = 1$, $l_z = 1$, $\Delta\varphi = -\pi/2$; (b) and (f) $l_y = 1$, $l_z = -1$, $\Delta\varphi = -\pi/2$; (c) and (g) $l_y = 1$, $l_z = -1$, $\Delta\varphi = 0$; (d) and (h) $l_y = 2$, $l_z = -1$, $\Delta\varphi = 0$. The electron number density $n_{0,0} = n_{\rm ini}\exp[-(r/r_{\rm CH})^6]$, where $n_{\rm ini} = 0.1n_c$ and $r_{\rm CH} = 4\lambda$. For all the lasers, $a_y = a_z = 0.2$ and $w_{0y} = w_{0z} = 4\lambda$.

propagates in the x direction with wavelength $\lambda = 1\ \mu$m. Its intensity remains constant after reaching the maximum $a_y = a_z = 0.2$ in three laser periods. The radius of the waist of the LG beams in the PIC simulations is $w_{0,y} = w_{0,z} = 4\ \mu$m. The simulation box is $10\ \mu\text{m}(x) \times 20\ \mu\text{m}(y) \times 20\ \mu\text{m}(z)$, with $500 \times 320 \times 320$ cells. For the electrons, 100 particles are applied per cell, and the ions are set to be immobile. The plasma is located at $2 < x < 8\ \mu$m. The distribution of the initial electron number density is $n_{0,0} = n_{\text{ini}} \exp[-(r/r_{\text{CH}})^6]$, where $n_{\text{ini}} = 0.1n_c$ and $r_{\text{CH}} = 4\lambda$. The initial electron temperature is 10 eV.

Figures 1(e)–1(h) show the transverse distributions of the quasi-static axial magnetic fields obtained in PIC simulations for different modes of lasers propagating in a plasma at $t = 66.67$ fs. The quasi-static magnetic fields and the related azimuthal currents are obtained by averaging the instantaneous magnetic fields and currents over two laser periods ($60 < t < 66.67$ fs) and then averaging along the laser propagation direction. The distributions of the axial magnetic fields given by the 3D PIC simulations shown in Figs. 1(e)–1(h) are quantitatively in good agreement with those given by the theoretical model in Figs. 1(a)–1(d).

Furthermore, we examine the theoretical model in detail by confirming the distribution of the azimuthal components of currents $\mathbf{J}_{nl}$ and $\mathbf{J}_{dm}$. The parameters are the same as those in Fig. 1(b). The theoretical $J^t_{nl,\theta}$ obtained from Eq. (14) and $J^t_{dm,\theta}$ calculated by $J^t_{dm,\theta} = -(1/\mu_0)\partial B_x/\partial r - J^t_{nl,\theta}$ are presented in Fig. 2(a) and 2(b). Figures 2(c) and 2(d) present the transverse distributions of $J^s_{nl,\theta}$ and $J^s_{dm,\theta}$ obtained in the corresponding PIC simulation of Fig. 1(f). $J^s_{dm,\theta}$ is diagnosed by $J^s_{dm,\theta} = \langle n^s_e \rangle \langle J^s_\theta / n^s_e \rangle$, where n^s_e and J^s_θ are the electron number density and the total azimuthal current in every simulation time step, respectively, and the angle brackets represent averaging over two laser periods (a total of 120 time steps). Then, $J^s_{nl,\theta}$ is obtained by $J^s_{nl,\theta} = \langle J^s_\theta \rangle - J^s_{dm,\theta}$. It is obvious that the theoretical results are in good agreement with those obtained from PIC simulations for both $J_{nl,\theta}$ and $J_{dm,\theta}$. In addition, the sign of $J_{dm,\theta}$ is always opposite to that of $J_{nl,\theta}$, as can be seen from a comparison of Fig. 2(c) and 2(d). This reflects the property of $\mathbf{J}_{dm}$ as a diamagnetic current.

The assumption of generalized vorticity conservation in the theoretical model can also be verified by the PIC simulations. This conservation law indicates that if the generalized vorticity is initially zero, $\boldsymbol{\omega} = 0$, it will remain zero throughout the subsequent evolution. In the PIC simulation setups, the initial zero-vorticity condition is satisfied. Therefore, the axial magnetic field can be calculated in another way by using the $\mathbf{u}_s$ given by the PIC simulations

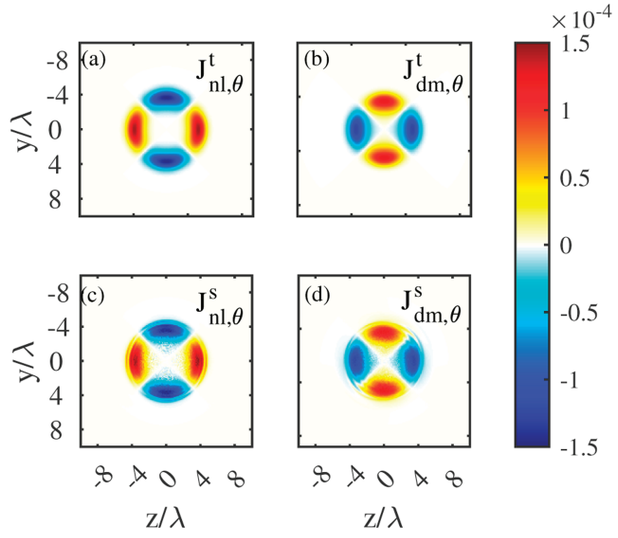

FIG. 2. Transverse distributions of different azimuthal currents (normalized by $J_0 = n_c ec$): (a) $J^t_{nl,\theta}$ from the theoretical model; (b) $J^t_{dm,\theta}$ from the theoretical model; (c) $J^s_{nl,\theta}$ from the PIC simulation; (d) $J^s_{dm,\theta}$ from the PIC simulation. The laser parameters are $l_y = 1$, $l_z = -1$, $\Delta\varphi = -\pi/2$, $a_y = a_z = 0.2$, and $w_{0y} = w_{0z} = 4\lambda$. The electron number density $n_{0,0} = n_{\text{ini}} \exp[-(r/r_{\text{CH}})^6]$, where $n_{\text{ini}} = 0.1n_c$ and $r_{\text{CH}} = 4\lambda$.

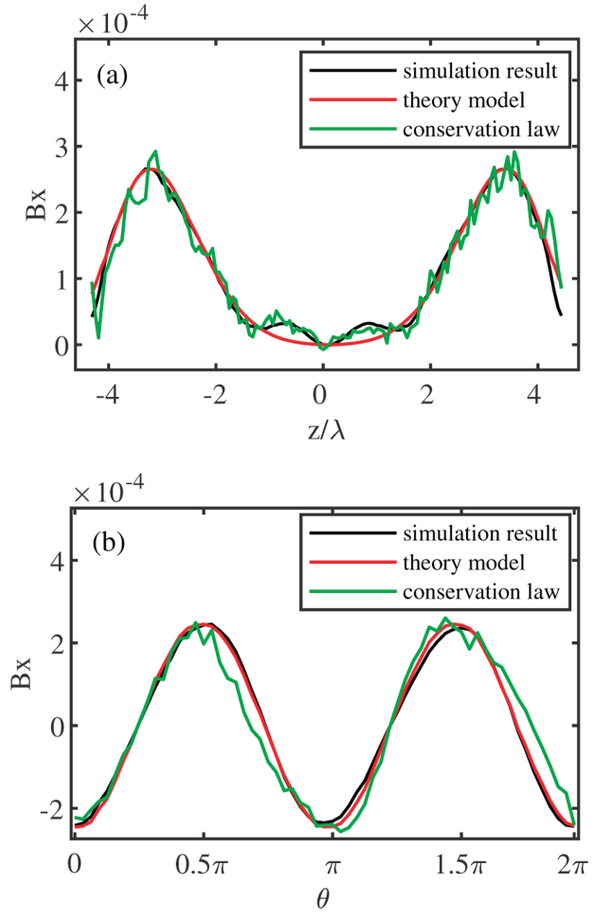

FIG. 3. Magnetic field (normalized by $B_0 = m_e\omega_0/e$) distributions (a) along $y = 0$ and (b) along θ at $r = 3\lambda$. The black line shows the results of the PIC simulations, the red line those of the theoretical model, and the green line those calculated from conservation of generalized vorticity. The laser parameters are $l_y = 1$, $l_z = -1$, $\Delta\varphi = -\pi/2$, $a_y = a_z = 0.2$, and $w_{0y} = w_{0z} = 4\lambda$. The electron number density $n_{0,0} = n_{\text{ini}} \exp[-(r/r_{\text{CH}})^6]$, where $n_{\text{ini}} = 0.1n_c$, and $r_{\text{CH}} = 4\lambda$.

through Eq. (10), in addition to the purely theoretical calculation using Eq. (11) and the direct diagnosis by PIC simulation as shown in Fig. 1. Figure 3 compares the axial magnetic fields obtained in these three ways. The black line shows the quasi-static magnetic field given directly by the PIC simulations, the red line shows the results from the theoretical model corresponding to those in Figs. 1(a)–1(d), and the green line shows the results calculated from conservation of generalized vorticity using the $\mathbf{u}_s$ data from the PIC simulations. It can be seen that the lines overlap well with each other, which proves good conservation of zero vorticity.

IV. DISCUSSION

We have constructed a self-consistent theoretical model for calculating the axial magnetic field induced by the nonlinear azimuthal current and the diamagnetic current. The soundness of this model has been comprehensively verified through 3D PIC simulations in terms of the distributions of magnetic fields and the source currents, as well as the conservation of generalized vorticity. Here, in the framework of the electron magnetic momentum model,[16] we present an intuitive explanation of why these magnetic fields vary with azimuth θ.

Figure 4(a) shows the intensity distribution on the focal plane for a laser with $l_y = 1$, $l_z = -1$, and $\Delta\varphi = -\pi/2$, together with the polarization state distribution marked by the small ellipses. The white and green ellipses represent left- and right-handed laser polarization states, respectively. The laser polarization changes azimuthally, which indicates different electron motions at different azimuths. Figures 4(b)–4(e) present the trajectories of electrons in this laser for one laser period T_0 near the red points in Fig. 4(a). The characteristic scale length of electron motion is about 0.06λ, which indicates that the electrons mainly move locally, owing to the relatively low laser intensity. On $\theta = \arctan(z/y) = \pi/4$ and $3\pi/4$, the laser can be regarded as linearly polarized, and the electrons oscillate along a certain direction [shown in Fig. 4(c) and 4(e)]. On $\theta = 0$ and $\pi/2$, the laser can be viewed as circularly polarized, and the electrons move circularly, as shown in Fig. 4(b) and 4(d). It is found that on $\theta = 0$, the direction of circular movement is opposite to that on $\theta = \pi/2$, which indicates that the directions of the magnetic fields generated by the magnetic dipole moments are opposite for $\theta = 0$ and $\theta = \pi/2$. The variation of the axial magnetic field on other azimuths can be analyzed similarly.

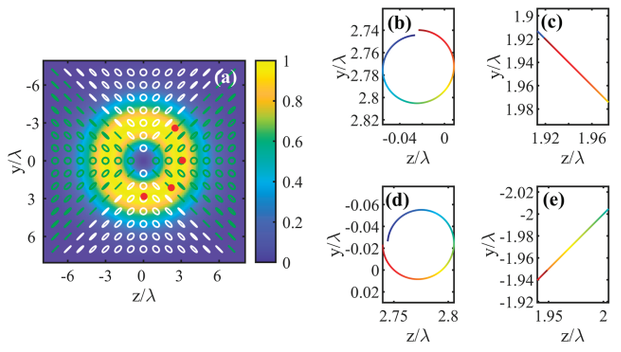

FIG. 4. (a) Distribution of laser intensity with laser parameters $l_y = 1$, $l_z = -1$, $\Delta\varphi = -\pi/2$, $a_y = a_z = 0.2$, and $w_{0y} = w_{0z} = 4\lambda$. White and green ellipses represent laser polarization states that are left- and right-handed, respectively. (b)–(e) Trajectories of electrons in this laser for one laser period near $(r, \theta) = (2.8\lambda, 0)$, $(2.8\lambda, \pi/4)$, $(2.8\lambda, \pi/2)$, and $(2.8\lambda, 3\pi/4)$, respectively, marked by the red points in (a). The color change from blue to red indicates the time evolution.

In addition to the polarization distribution, Eq. (11) implies that the initial density distribution n_s also plays a role. As well as the super-Gaussian density distribution $n_{0,0}$ applied above, another two density profiles are also studied, and the axial magnetic fields generated are shown in Fig. 5. One density profile is a plasma channel, $n_{0,1} = n_{\rm ini}\{1 - \exp[-(r/r_{\rm CH})^6]\}$, and the other is the previous super-Gaussian density distribution superimposed on a uniform background, $n_{0,2} = n_{\rm ini}\{0.5 + \exp[-(r/r_{\rm CH})^6]\}$. The other plasma and laser parameters are the same as those in Fig. 1(b). These results reveal that the theory and simulation results are in good agreement.

Note that the density gradient of $n_{0,1}$ is opposite to that of $n_{0,0}$, and so the corresponding nonlinear current $j_{nl,\theta}$ is opposite according to Eq. (14), which is verified by the red solid and red dotted lines in Fig. 6. However, the magnetic field distributions in the two cases are quite similar, as can be seen by comparing Fig. 1(b) and 5(a). This suggests that the characteristics of the generated magnetic fields cannot be determined only by $j_{nl,\theta}$, and the diamagnetic currents $j_{dm,\theta}$ should also be taken into account. The green solid and green dotted lines in Fig. 6 show $j_{dm,\theta}$ corresponding to these two cases. It can be seen that $j_{dm,\theta}$ in the $n_{0,0}$ case peaks at $r < r_{\rm CH}$, whereas it peaks at $r > r_{\rm CH}$ in the $n_{0,1}$ case. This leads to a similar sinusoidal-like distribution of the total azimuthal current along r in both cases, as shown by the black solid and black dotted lines in Fig. 6. Considering

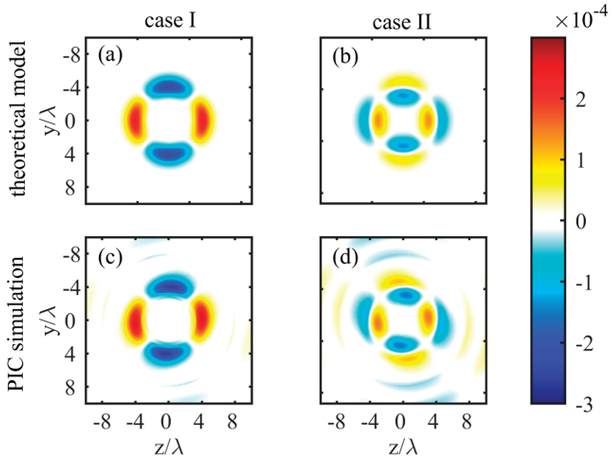

FIG. 5. Transverse distributions of the quasi-static axial self-generated magnetic fields (normalized by $B_0 = m_e\omega_0/e$) for different electron number density distributions: (a) and (c) $n_{0,1} = n_{\rm ini}\{1 - \exp[-(r/r_{\rm CH})^6]\}$; (b) and (d) $n_{0,2} = n_{\rm ini}\{0.5 + \exp[-(r/r_{\rm CH})^6]\}$. Here, $n_{\rm ini} = 0.1n_c$ and $r_{\rm CH} = 4\lambda$. (a) and (b) show the results from the theoretical model, and (c) and (d) show the results from the 3D PIC simulations. The laser parameters are $l_y = 1$, $l_z = -1$, $\Delta\varphi = -\pi/2$, $a_y = a_z = 0.2$, and $w_{0y} = w_{0z} = 4\lambda$.

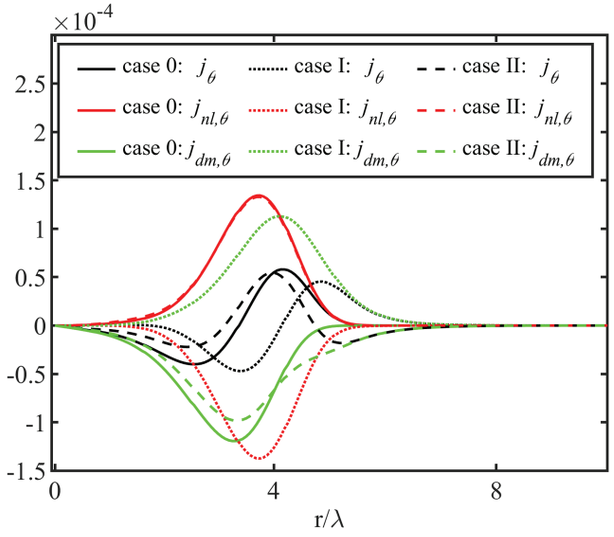

FIG. 6. Distributions of different azimuthal currents (normalized by $J_0 = n_c ec$) along r at $\theta = \pi/2$ ($y = 0$, $z > 0$) obtained from the theoretical model. The solid lines (case 0) show the results with the density profile $n_{0,0} = n_{\rm ini}\exp[-(r/r_{\rm CH})^6]$, the dotted lines (case I) the results with the profile $n_{0,1} = n_{\rm ini}\{1-\exp[-(r/r_{\rm CH})^6]\}$, and the dashed lines the results with the profile $n_{0,2} = n_{\rm ini}\{0.5+\exp[-(r/r_{\rm CH})^6]\}$. The red lines show the source current $j_{nl,\theta}$, the green lines the diamagnetic current $j_{dm,\theta}$, and the black lines the total azimuthal current $j_\theta = j_{nl,\theta} + j_{dm,\theta}$. The plasma parameters are $n_{\rm ini} = 0.1n_c$ and $r_{\rm CH} = 4\lambda$. The laser parameters are $l_y = 1$, $l_z = -1$, $\Delta\varphi = -\pi/2$, $a_y = a_z = 0.2$, and $w_{0y} = w_{0z} = 4\lambda$.

that the magnetic field can be calculated as $B_x = \mu_0\int_r^\infty j_\theta\, dr$, it is no wonder that the distribution of the magnetic field is similar rather than opposite for these two cases. Likewise, although $j_{nl,\theta}$ is predicted to be the same for the $n_{0,2}$ and $n_{0,0}$ cases (as demonstrated by the overlap of the red solid and red dashed lines in Fig. 6), the generated magnetic field distribution is rather different, because the distribution of the diamagnetic current depends on the different initial density profiles.

Such unique distributions of axial magnetic fields provide a new azimuthal degree of freedom in designing magnetized plasma-based devices.[37,46] It can be proved that, in principle, arbitrary distributions of axial magnetic fields in the azimuthal direction can be generated. Since the electromagnetic waves are weakly relativistic, the relativistic factor can be approximated as $\gamma_0 = \sqrt{1+|E_L|^2/2E_0^2} \approx 1$. If the initial electron density gradient is large enough, then $\partial n_s/\partial r \approx \partial n_0/\partial r$. Equation (14) can then be rewritten as

$$\mathbf{J}_{nl} = -\frac{e^3E_0^2a_ya_zh_y(r)h_z(r)}{2m_e^2\omega_0^3}\frac{\partial n_0}{\partial r}\sin(\theta\Delta l+\Delta\varphi)\,\mathbf{e}_\theta. \qquad (15)$$

By setting $E_z^{LG}/E_0 = a_zh_z(r)\exp(il_z\theta+i\varphi_z)$ and $E_y^{LG}/E_0 = \sum_m a_{y,m}h_{y,m}(r)\exp(il_{y,m}\theta+i\varphi_{y,m})$, where $m = 0,\pm1,\pm2,\ldots$, we can obtain $\mathbf{J}_{nl} = \sum_m J_{nl,m}\sin(\Delta l_m\theta+\Delta\varphi_m)\mathbf{e}_\theta$, where

$$J_{nl,m} = -\frac{e^3E_0^2a_{y,m}a_zh_{y,m}(r)h_z(r)}{2m_e^2\omega_0^3}\frac{\partial n_0}{\partial r},$$
$$\Delta l_m = l_{y,m}-l_z, \qquad \Delta\varphi_m = \varphi_{y,m}-\varphi_z.$$

This indicates that any azimuthally varying distribution of $\mathbf{J}_{nl}$ can be designed with a proper combination of Δl and $\Delta\varphi$, and the corresponding axial magnetic field can be manipulated.

As a coda, we present the ladybug-like magnetic field shown in Fig. 7. It is generated by the above method using a laser with $E_z^{LG}/E_0 = a_zh_z(r)\exp(-i\theta)$ and $E_y^{LG}/E_0 = a_{y,1}h_{y,1}(r)\exp(i\theta) + a_{y,2}h_{y,2}(r)\exp(2i\theta)$. In a similar way, more complex distributions of axial magnetic field could, in principle, be designed.

It is worth noting that the results given by the theoretical model are in good agreement with those given by PIC simulations, which can be mainly attributed to three factors. First, laser absorption is negligible in our weakly relativistic (5×10^{16} W/cm^2) laser plasma interaction, where the effects of collisions and parametric instabilities are neglected. Thus, AM absorption, which plays a dominant role in Refs. 29, 30, and 39, is not of concern. If the AM absorption is significant, the electrons can acquire an appreciable low-frequency velocity $\mathbf{u}_s$. The corresponding current $\mathbf{J} = -en_s\mathbf{u}_s$ will then be another key source for the magnetic field, and the related magnetic fields depend strongly on the specific AM absorption mechanism, which is not considered in our model. Second, the ion motions are neglected in our discussion, since our model is applicable on a time scale of $\omega_{pe}^{-1} < \tau < \omega_{pi}^{-1}$. It can be anticipated that for a longer time $\tau > \omega_{pi}^{-1}$, the ion motions under the charge-separation field might change the transverse density distribution of the plasma and result in different magnetic field distributions according to our analysis. Finally, our model is based on the assumption of a cold plasma. If thermal effects are not negligible, then kinetic models[48,49]

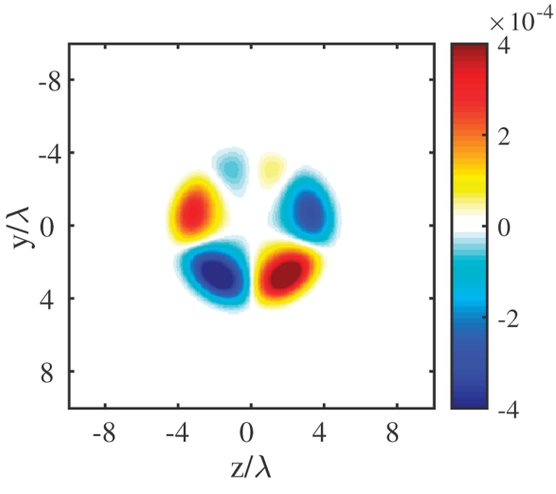

FIG. 7. Distribution of the axial magnetic field (normalized by $B_0 = m_e\omega_0/e$) obtained from the theoretical model for a laser with $E_z^{LG}/E_0 = a_zh_z(r)\exp(-i\theta)$ and $E_y^{LG}/E_0 = a_{y,1}h_{y,1}(r)\exp(i\theta) + a_{y,2}h_{y,2}(r)\exp(2i\theta)$. The laser parameters are $a_z = a_{y,1} = a_{y,2} = 0.2$ and $w_z = w_{y,1} = w_{y,2} = 4\lambda$. The electron number density $n_{0,0} = n_{\rm ini}\exp[-(r/r_{\rm CH})^6]$, where $n_{\rm ini} = 0.1n_c$ and $r_{\rm CH} = 4\lambda$.

or the ten-moment Grad system of hydrodynamic equations[50] are needed for the analysis, which is beyond the scope of this work.

V. CONCLUSION

The inverse Faraday effect has been extended to full Poincaré beams, and a novel scheme for generating azimuthally dependent axial magnetic fields has been proposed. Starting from fluid theory and conservation of generalized vorticity, we have constructed an integrated theoretical model of the quasi-static magnetic field generated by both the nonlinear azimuthal current and the diamagnetic current. This model predicts that the self-generated axial magnetic field varies azimuthally for a full Poincaré beam propagating in a plasma. The structures of such magnetic fields are determined by the Laguerre–Gaussian mode difference Δl and the initial phase difference $\Delta\varphi$ of the composing orthogonally polarized lasers. Three-dimensional particle-in-cell simulation results are in good agreement with the theoretical model both qualitatively and quantitatively. In addition, it is noted that an arbitrary azimuthally varying distribution of the axial magnetic field can be obtained by the linear superposition method, which provides a potential new azimuthal degree of freedom in the design of magnetized plasma devices.

ACKNOWLEDGMENTS

This research was supported by the National Natural Science Foundation of China (NSFC) under Grant No. 11975014 and by the Strategic Priority Research Program of Chinese Academy of Sciences under Grant Nos. XDA25050400 and XDA25010200. The numerical calculations in this paper were performed on the supercomputing system at the Supercomputing Center of the University of Science and Technology of China.

AUTHOR DECLARATIONS

Conflict of Interest

The authors have no conflicts to disclose.

Author Contributions

Wei Liu: Visualization (lead); Writing – original draft (lead). **Qing Jia**: Funding acquisition (lead); Writing – review & editing (lead). **Jian Zheng**: Writing – review & editing (supporting).

DATA AVAILABILITY

The data that support the findings of this study are available within the article.

APPENDIX: SIMULATION RESULTS OF WEAKLY RELATIVISTIC GAUSSIAN AND LG BEAMS

PIC simulations of weakly relativistic Gaussian beam plasma interactions were performed. A comparison of the theoretical and simulation results for the magnetic field is shown in Fig. 8. The overlap between the red and black lines demonstrates the good fit between our theory and the simulation. A comparison of the blue and red lines reveals an opposite magnetic field for different circularly polarized (CP) Gaussian beams when other parameters are the same. The green line shows that the self-generated magnetic field of an linearly polarized (LP) Gaussian beam is negligible compared with the case of circular polarization. These results are consistent with theoretical expectations. For a benchmark, the electron number density is set as $n_{0,3} = n_{\mathrm{ini}}/[1 + 9\exp(-r^2/r_{\mathrm{CH}}^2)]$, the same as in Ref. 21, and the magnetic field distribution shown in Fig. 8 is in agreement with that in Ref. 21.

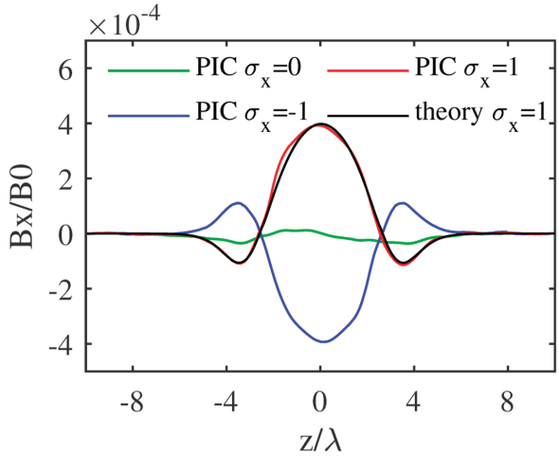

FIG. 8. Distributions of axial magnetic fields (normalized by $B_0 = m_e\omega_0/e$) along $y = 0$ generated by different polarized Gaussian beams. The red and blue lines show the results of PIC simulation for right- and left-hand ($\sigma_x = \pm 1$) circularly polarized lasers, respectively, the black line shows the result of the theoretical model for a right-hand ($\sigma_x = 1$) circularly polarized laser, and the green line shows the result of PIC simulation for a linearly ($\sigma_x = 0$) polarized laser. The laser parameters are $a_0 = 0.3$ and $w_0 = 4\lambda$. The plasma has $n_{0,3} = n_{\mathrm{ini}}/[1 + 9\exp(-r^2/r_{\mathrm{CH}}^2)]$, where $n_{\mathrm{ini}} = 0.1n_c$ and $r_{\mathrm{CH}} = 2\lambda$.

To further verify that the angular momentum transfer mechanism can be ignored in our simulations, three comparative simulations of the interaction of two CP LG beams ($l = \pm 1$, $\sigma_x = -1$) and one LP LG beam ($l = 1$, $\sigma_x = 0$) with the same plasma were performed. The simulation results for the quasi-static magnetic field distributions are shown in Fig. 9. Our beating current model predicts the same magnetic field distribution for the two CP beam cases, given the same polarization ($\sigma_x = -1$) and intensity. This is confirmed by the overlap of the red and black lines shown in Fig. 9. By contrast, the angular momentum transfer model[22,23] predicts that the magnetic fields for these two CP beams are very different, given the different OAM distributions ($l = \pm 1$) and the total angular momentum ($l + \sigma_x = -2, 0$). Moreover, a direct proof can be obtained by comparing the green and black lines, which shows that the magnetic field generated by the LP LG beam is negligible. All the above comparisons imply that there is negligible angular momentum transfer in our weakly relativistic laser plasma interaction process.

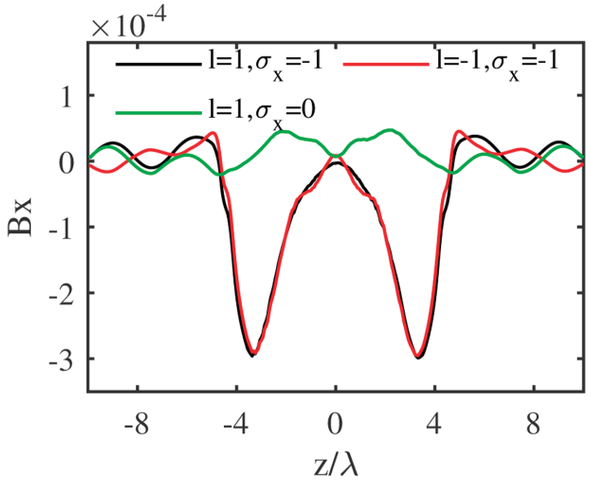

FIG. 9. Distributions of axial magnetic fields (normalized by $B_0 = m_e\omega_0/e$) along $y = 0$ generated by different LG lasers in PIC simulations. The black, red, and green lines represent the cases of a left-hand CP ($\sigma_x = -1$) LG laser with $l = 1$, a left-hand CP ($\sigma_x = -1$) LG laser with $l = -1$, and a LP ($\sigma_x = 0$) LG laser with $l = 1$, respectively. The other laser parameters are $a_0 = 0.2$ and $w_0 = 4\lambda$. The electron number density $n_{0,0} = n_{ini}\exp[-(r/r_{CH})^6]$, where $n_{ini} = 0.1n_c$ and $r_{CH} = 4\lambda$.

REFERENCES

[1]M. Tanimoto, S. Kato, E. Miura, N. Saito, K. Koyama, and J. K. Koga, "Direct electron acceleration by stochastic laser fields in the presence of self-generated magnetic fields," Phys. Rev. E **68**, 026401 (2003).

[2]X. H. Yuan, A. P. L. Robinson, M. N. Quinn, D. C. Carroll, M. Borghesi, R. J. Clarke, R. G. Evans, J. Fuchs, P. Gallegos, L. Lancia, D. Neely, K. Quinn, L. Romagnani, G. Sarri, P. A. Wilson, and P. McKenna, "Effect of self-generated magnetic fields on fast-electron beam divergence in solid targets," New J. Phys. **12**, 063018 (2010).

[3]B. Liu, H. Y. Wang, J. Liu, L. B. Fu, Y. J. Xu, X. Q. Yan, and X. T. He, "Generating overcritical dense relativistic electron beams via self-matching resonance acceleration," Phys. Rev. Lett. **110**, 045002 (2013).

[4]Z. Gong, F. Mackenroth, T. Wang, X. Q. Yan, T. Toncian, and A. V. Arefiev, "Direct laser acceleration of electrons assisted by strong laser-driven azimuthal plasma magnetic fields," Phys. Rev. E **102**, 013206 (2020).

[5]D. J. Stark, T. Toncian, and A. V. Arefiev, "Enhanced multi-MeV photon emission by a laser-driven electron beam in a self-generated magnetic field," Phys. Rev. Lett. **116**, 185003 (2016).

[6]M. A. Yates, D. B. van Hulsteyn, H. Rutkowski, G. Kyrala, and J. U. Brackbill, "Experimental evidence for self-generated magnetic fields and remote energy deposition in laser-irradiated targets," Phys. Rev. Lett. **49**, 1702–1704 (1982).

[7]M. Tabak, J. Hammer, M. E. Glinsky, W. L. Kruer, S. C. Wilks, J. Woodworth, E. M. Campbell, M. D. Perry, and R. J. Mason, "Ignition and high gain with ultrapowerful lasers," Phys. Plasmas **1**, 1626–1634 (1994).

[8]R. Kodama, P. A. Norreys, K. Mima, A. E. Dangor, R. G. Evans, H. Fujita, Y. Kitagawa, K. Krushelnick, T. Miyakoshi, N. Miyanaga, T. Norimatsu, S. J. Rose, T. Shozaki, K. Shigemori, A. Sunahara, M. Tampo, K. A. Tanaka, Y. Toyama, T. Yamanaka, and M. Zepf, "Fast heating of ultrahigh-density plasma as a step towards laser fusion ignition," Nature **412**, 798–802 (2001).

[9]H.-b. Cai, S. P. Zhu, M. Chen, S.-z. Wu, X. T. He, and K. Mima, "Magnetic-field generation and electron-collimation analysis for propagating fast electron beams in overdense plasmas," Phys. Rev. E **83**, 036408 (2011).

[10]W. A. Farmer, J. M. Koning, D. J. Strozzi, D. E. Hinkel, L. F. Berzak Hopkins, O. S. Jones, and M. D. Rosen, "Simulation of self-generated magnetic fields in an inertial fusion hohlraum environment," Phys. Plasmas **24**, 052703 (2017).

[11]E. M. Epperlein and M. G. Haines, "Plasma transport coefficients in a magnetic field by direct numerical solution of the Fokker–Planck equation," Phys. Fluids **29**, 1029–1041 (1986).

[12]Q. Jia, K. Mima, H.-b. Cai, T. Taguchi, H. Nagatomo, and X. T. He, "Self-generated magnetic dipoles in weakly magnetized beam-plasma system," Phys. Rev. E **91**, 023107 (2015).

[13]J. M. Tian, H. B. Cai, W. S. Zhang, E. H. Zhang, B. Du, and S. P. Zhu, "Generation mechanism of 100 MG magnetic fields in the interaction of ultra-intense laser pulse with nanostructured target," High Power Laser Sci. Eng. **8**, E16 (2020).

[14]H.-b. Cai, X.-x. Yan, P.-l. Yao, and S.-p. Zhu, "Hybrid fluid–particle modeling of shock-driven hydrodynamic instabilities in a plasma," Matter Radiat. Extremes **6**, 035901 (2021).

[15]J. Deschamps, M. Fitaire, and M. Lagoutte, "Inverse Faraday effect in a plasma," Phys. Rev. Lett. **25**, 1330–1332 (1970).

[16]A. D. Steiger and C. H. Woods, "Intensity-dependent propagation characteristics of circularly polarized high-power laser radiation in a dense electron plasma," Phys. Rev. A **5**, 1467–1474 (1972).

[17]Z. M. Sheng and J. Meyer-ter-Vehn, "Inverse Faraday effect and propagation of circularly polarized intense laser beams in plasmas," Phys. Rev. E **54**, 1833–1842 (1996).

[18]V. I. Berezhiani, S. M. Mahajan, and N. L. Shatashvili, "Theory of magnetic field generation by relativistically strong laser radiation," Phys. Rev. E **55**, 995–1001 (1997).

[19]A. Kim, M. Tushentsov, D. Anderson, and M. Lisak, "Axial magnetic fields in relativistic self-focusing channels," Phys. Rev. Lett. **89**, 095003 (2002).

[20]A. A. Frolov, "Excitation of magnetic fields by a circularly polarized laser pulse in a plasma channel," Plasma Phys. Rep. **30**, 698–709 (2004).

[21]N. Naseri, V. Y. Bychenkov, and W. Rozmus, "Axial magnetic field generation by intense circularly polarized laser pulses in underdense plasmas," Phys. Plasmas **17**, 083109 (2010).

[22]S. Ali, J. R. Davies, and J. T. Mendonca, "Inverse Faraday effect with linearly polarized laser pulses," Phys. Rev. Lett. **105**, 035001 (2010).

[23]M. G. Haines, "Generation of an axial magnetic field from photon spin," Phys. Rev. Lett. **87**, 135005 (2001).

[24]Z. Najmudin, M. Tatarakis, A. Pukhov, E. L. Clark, R. J. Clarke, A. E. Dangor, J. Faure, V. Malka, D. Neely, M. I. K. Santala, and K. Krushelnick, "Measurements of the inverse Faraday effect from relativistic laser interactions with an underdense plasma," Phys. Rev. Lett. **87**, 215004 (2001).

[25]I. Y. Kostyukov, G. Shvets, N. J. Fisch, and J. M. Rax, "Magnetic-field generation and electron acceleration in relativistic laser channel," Phys. Plasmas **9**, 636–648 (2002).

[26]G. Shvets, N. J. Fisch, and J. M. Rax, "Magnetic field generation through angular momentum exchange between circularly polarized radiation and charged particles," Phys. Rev. E **65**, 046403 (2002).

[27]D. Wu and J. W. Wang, "Magetostatic amplifier with tunable maximum by twisted-light plasma interactions," Plasma Phys. Controlled Fusion **59**, 095010 (2017).

[28]Y. Shi, J. Vieira, R. M. G. M. Trines, R. Bingham, B. F. Shen, and R. J. Kingham, "Magnetic field generation in plasma waves driven by copropagating intense twisted lasers," Phys. Rev. Lett. **121**, 145002 (2018).

[29]R. Nuter, P. Korneev, I. Thiele, and V. Tikhonchuk, "Plasma solenoid driven by a laser beam carrying an orbital angular momentum," Phys. Rev. E **98**, 033211 (2018).

[30]A. Longman and R. Fedosejevs, "Kilo-Tesla axial magnetic field generation with high intensity spin and orbital angular momentum beams," Phys. Rev. Res. **3**, 043180 (2021).

[31]R. N. Sudan, "Mechanism for the generation of 10^9 G magnetic fields in the interaction of ultraintense short laser pulse with an overdense plasma target," Phys. Rev. Lett. **70**, 3075–3078 (1993).

[32]R. A. Beth, "Mechanical detection and measurement of the angular momentum of light," Phys. Rev. **50**, 115–125 (1936).
[33]L. Allen, M. W. Beijersbergen, R. J. C. Spreeuw, and J. P. Woerdman, "Orbital angular momentum of light and the transformation of Laguerre-Gaussian laser modes," Phys. Rev. A **45**, 8185–8189 (1992).
[34]Y. Shi, B. Shen, L. Zhang, X. Zhang, W. Wang, and Z. Xu, "Light fan driven by a relativistic laser pulse," Phys. Rev. Lett. **112**, 235001 (2014).
[35]J. Vieira, R. M. G. M. Trines, E. P. Alves, R. A. Fonseca, J. T. Mendonça, R. Bingham, P. Norreys, and L. O. Silva, "Amplification and generation of ultra-intense twisted laser pulses via stimulated Raman scattering," Nat. Commun. **7**, 10371 (2016).
[36]A. Leblanc, A. Denoeud, L. Chopineau, G. Mennerat, P. Martin, and F. Quéré, "Plasma holograms for ultrahigh-intensity optics," Nat. Phys. **13**, 440–443 (2017).
[37]K. Qu, Q. Jia, and N. J. Fisch, "Plasma *q*-plate for generation and manipulation of intense optical vortices," Phys. Rev. E **96**, 053207 (2017).
[38]W. P. Wang, C. Jiang, H. Dong, X. M. Lu, J. F. Li, R. J. Xu, Y. J. Sun, L. H. Yu, Z. Guo, X. Y. Liang, Y. X. Leng, R. X. Li, and Z. Z. Xu, "Hollow plasma acceleration driven by a relativistic reflected hollow laser," Phys. Rev. Lett. **125**, 034801 (2020).
[39]R. Nuter, P. Korneev, E. Dmitriev, I. Thiele, and V. T. Tikhonchuk, "Gain of electron orbital angular momentum in a direct laser acceleration process," Phys. Rev. E **101**, 053202 (2020).
[40]A. M. Beckley, T. G. Brown, and M. A. Alonso, "Full Poincaré beams," Opt. Express **18**, 10777–10785 (2010).
[41]L.-G. Wang, "Optical forces on submicron particles induced by full Poincaré beams," Opt. Express **20**, 20814–20826 (2012).
[42]W. Zhu, V. Shvedov, W. She, and W. Krolikowski, "Transverse spin angular momentum of tightly focused full Poincaré beams," Opt. Express **23**, 34029–34041 (2015).
[43]W. Lin, Y. Ota, Y. Arakawa, and S. Iwamoto, "Microcavity-based generation of full Poincaré beams with arbitrary skyrmion numbers," Phys. Rev. Res. **3**, 023055 (2021).
[44]C. Thaury, F. Quéré, J.-P. Geindre, A. Levy, T. Ceccotti, P. Monot, M. Bougeard, F. Réau, P. d'Oliveira, P. Audebert, R. Marjoribanks, and P. Martin, "Plasma mirrors for ultrahigh-intensity optics," Nat. Phys. **3**, 424–429 (2007).
[45]S. Monchocé, S. Kahaly, A. Leblanc, L. Videau, P. Combis, F. Réau, D. Garzella, P. D'Oliveira, P. Martin, and F. Quéré, "Optically controlled solid-density transient plasma gratings," Phys. Rev. Lett. **112**, 145008 (2014).
[46]S. Weng, Q. Zhao, Z. Sheng, W. Yu, S. Luan, M. Chen, L. Yu, M. Murakami, W. B. Mori, and J. Zhang, "Extreme case of Faraday effect: Magnetic splitting of ultrashort laser pulses in plasmas," Optica **4**, 1086–1091 (2017).
[47]T. D. Arber, K. Bennett, C. S. Brady, A. Lawrence-Douglas, M. G. Ramsay, N. J. Sircombe, P. Gillies, R. G. Evans, H. Schmitz, A. R. Bell, and C. P. Ridgers, "Contemporary particle-in-cell approach to laser-plasma modelling," Plasma Phys. Controlled Fusion **57**, 113001 (2015).
[48]S.-p. Zhu, C. Y. Zheng, and X. T. He, "A theoretical model for a spontaneous magnetic field in intense laser plasma interaction," Phys. Plasmas **10**, 4166–4168 (2003).
[49]B. Qiao, S.-p. Zhu, C. Y. Zheng, and X. T. He, "Quasistatic magnetic and electric fields generated in intense laser plasma interaction," Phys. Plasmas **12**, 053104 (2005).
[50]B. Qiao, X. T. He, and S.-p. Zhu, "Fluid theory for quasistatic magnetic field generation in intense laser plasma interaction," Phys. Plasmas **13**, 053106 (2006).